

A Finite-Time Quantum Otto Engine subject to Control Noise and Enhancement Techniques

Theodore McKeever, Owen Diba, and Ahsan Nazir

Department of Physics and Astronomy, The University of Manchester, Manchester M13 9PL, UK.

(Dated: December 20, 2024)

With the development of any quantum technology comes a need for precise control of quantum systems. Here, we evaluate the impact of control noise on a quantum Otto cycle. Whilst it is postulated that noiseless quantum engines can approach maximal Otto efficiency in finite times, the existence of white noise on the controls is shown to negatively affect average engine performance. Two methods of quantum enhancement, counterdiabatic driving and quantum lubrication, are implemented and found to improve the performance of the noisy cycle only in specified parameter regimes. To gain insight into performance fluctuations, projective energy measurements are used to construct a noise-averaged probability distribution without assuming full thermalisation or adiabaticity. From this, the variances in thermodynamic currents are observed to increase as average power and efficiency improve, and are also shown to be consistent with known bounds from thermodynamic uncertainty relations. Lastly, by comparing the average functioning of the unmonitored engine to a projectively-measured engine cycle, the role of coherence in work extraction for this quantum engine model is investigated.

I. INTRODUCTION

The study of quantum engines is well established [1–5], providing useful theoretical frameworks to test the consistency of quantum and classical thermodynamics. For instance, the relationship between quantum and classical definitions of adiabaticity can also be viewed through the lens of quantum heat engines where the inclination of a quantum system to remain in its instantaneous eigenstate [6] directly influences the efficiency of the system operation. Quantum engines enable investigation into some unique features of thermodynamics in the quantum regime, such as overcoming classical performance trade-offs [7] and the implementation of quantum enhancement techniques, both of which are addressed in this work. With recent physical realisations of quantum heat engines [8–11], there is also potential for functional applications, acting as sources of power for components within other quantum technologies. A cyclic heat engine operating in reverse functions as a refrigerator. Thus the findings presented here also apply indirectly to the performance of quantum refrigerators, which have a number of potential applications where reaching extremely cool and stable temperatures is required [12–15].

The presence of control noise is inevitable whenever classical technology is used to generate controls. Therefore, the inclusion of noisy parameters in quantum control is necessary in providing a complete analysis of any driven quantum system or realised quantum technology. Further, not just in practice but in principle, it has been posited that noise is fundamental to the interaction between quantum and classical objects due to the back-reaction of quantum systems on classical influences [16]. In which case, accounting for control noise is vital for any theoretical model of a driven quantum system. The quantum engine analysed in this paper thus constitutes an open quantum system combining the influences of noisy driving protocols and weak coupling to a thermal bath.

The utility of a quantum machine, like a classical machine, can be defined by its ability to complete a specific task. For instance, the charging of a battery by a (quantum) heat engine or the heat extraction from a cold bath by a (quantum) refrigerator. Such tasks often require the completion of several cycles. Therefore, the performance of quantum machines is commonly taken over many consecutive operations, where fluctuations are not usually considered and the cumulative action (some overall change in a thermodynamic observable) is measured [17]. This cycle is then repeated and divided by the number of cycle repetitions per experiment to calculate the average performance per cycle. In such cases, we calculate the average performance of a noisy quantum Otto engine using non-invasive energy expectation values. On the other hand, the full probability distribution is also valuable as it contains information on both average performance and fluctuations, and is particularly relevant, for example, under circumstances where quantum machines are needed only in short bursts with minimal consecutive operations. To construct the probability distribution for the quantum Otto engine, we probe the internal state of the working substance (a qubit) by subjecting it to projective energy measurements. Such measurements destroy coherence in the quantum system. Therefore, as well as accessing higher-order performance statistics for individual cycles, we are able to compute the role of coherence in the quantum engine by comparing results from projective measurements versus non-invasive expectation values.

The paper is organised as follows. In Section II we introduce the engine model under review, including details of the cycle strokes and the existence of a limit cycle. Following this, in Section III, we raise the distinction between heat and work for noisy control. We then implement methods of performance enhancement within the quantum regime in Section IV, and assess the average performance of the engine with and without such tech-

niques in Section V. Next, we calculate the full probability distribution of an equivalent engine using invasive energy measurements within the cycle. From this, we deduce the expected performance and its variance in Section VI, before summarising and drawing our conclusions in Section VII.

II. ENGINE MODEL

A. The Quantum Otto Cycle

In parallel to their classical counterparts, there are several types of quantum engines operating either continuously [18] or in a reciprocating cycle. The Otto engine is a paradigmatic example of the latter, consisting of four strokes: two isentropes and two isochores, performed cyclically. Each stroke $a \rightarrow b$ has an allocated time τ_{ab} which for the remainder of this work are taken to be equal to each other. Explicitly, the stages (illustrated in Figure 1) are as follows:

0 \rightarrow 1: Compression. On this isentrope, work is done on the system (W_{01}), altering the system Hamiltonian from $H_C \rightarrow H_H$, increasing the difference between energy eigenvalues, $\Omega_C \rightarrow \Omega_H$ as in Equations 1 and 2 below.

1 \rightarrow 2: Heating. On this isochore, the system is coupled to the hot bath at inverse temperature β_H , absorbing heat Q_H whilst the Hamiltonian is kept constant, H_H .

2 \rightarrow 3: Expansion. On this isentrope, work is done by the system ($-W_{23}$), altering the system Hamiltonian from $H_H \rightarrow H_C$, which decreases the difference between energy eigenvalues, $\Omega_H \rightarrow \Omega_C$.

3 \rightarrow 0: Cooling. On this isochore, the system is coupled to the cold bath at inverse temperature β_C , releasing heat Q_C whilst the Hamiltonian is kept constant, H_C .

B. Open Quantum Dynamics

The working substance of the quantum Otto engine is taken to be a two-level system with intrinsic (and constant) tunnelling, $\Omega_x \sigma_x$, and with an applied external control field providing a time-dependent energy level splitting, $\Omega_z(t) \sigma_z$, which could describe, for instance, a trapped ion with energy level splitting controlled by laser pulses, or a quantum dot driven by an electromagnetic field. This set-up gives rise to the system Hamiltonian:

$$H_S(t) = \frac{1}{2} (\Omega(t) \mathbb{1} + \Omega_x \sigma_x + \Omega_z(t) \sigma_z) \quad (1)$$

with eigenvalues $\Omega(t)$ and 0, where $\Omega(t) = \sqrt{\Omega_x^2 + \Omega_z(t)^2}$. $H_S(t)$ can be represented in its energy eigenbasis (we denote any operator in this basis

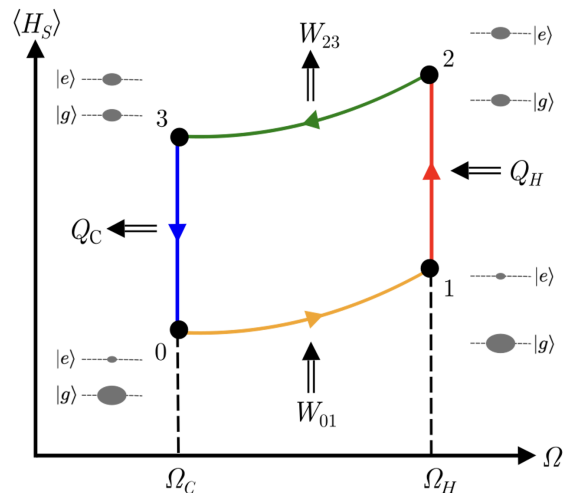


Figure 1. In the 4-stroke Otto engine, the system exchanges heat Q_i ($i = H, C$) with a bath at inverse temperature β_i , along the isochores (Red, Blue). Work W_{01} is performed on the system during isentropic compression (Orange) and work W_{23} is extracted from the engine during isentropic expansion (Green). Ω represents the energy splitting of the system and $\langle H_S \rangle$ represents the expectation value of the internal energy of the system. Approximate energy level diagrams are given for each cycle vertex, showing the change in populations and energy level splitting in the energy eigenbasis $\{|e\rangle, |g\rangle\}$.

by a prime) by rotating with $R(t) = e^{-i\theta(t)\sigma_y/2}$, where $\theta(t) = \arctan(\Omega_x/\Omega_z(t))$:

$$H'_S(t) = R^\dagger(t)H_S(t)R(t) = \begin{pmatrix} \Omega(t) & 0 \\ 0 & 0 \end{pmatrix}. \quad (2)$$

The system is driven between $H_C \leftrightarrow H_H$ as $\Omega_z(t)$ is varied. A polynomial ansatz is used for the sweeping of $\Omega_z(t)$ such that it varies smoothly across the isentropes between $\Omega_{z,C} \leftrightarrow \Omega_{z,H}$ with a zero time-derivative at the beginning and end of each stroke. In terms of dimensionless time, $s_{ab} = t_{ab}/\tau_{ab}$, over an isentrope $a \rightarrow b$, the form of the external driving is given by $\Omega_z(t) = (3s_{ab}^2 - 2s_{ab}^3)(\Omega_z^b - \Omega_z^a) + \Omega_z^a$ where Ω_z^a (Ω_z^b) is the chosen value of Ω_z at the beginning (end) of the stroke.

Along the isochores, the hot and cold thermal reservoirs can be modelled as large, memoryless bosonic baths weakly interacting with a static system:

$$H_T = H_S + H_B + H_I \\ = H_S + \sum_k \omega_k b_k^\dagger b_k + \sigma_z \otimes \sum_k g_k (b_k^\dagger + b_k). \quad (3)$$

Here H_B is given as a sum of quantum harmonic oscillators [19], where b_k^\dagger and b_k are the raising and lowering operators of the bath modes with frequencies ω_k , which couple to the system with strengths g_k .

Within the Born-Markov approximations, the von Neumann equation $\dot{\rho}(t) = -i[H(t), \rho(t)]$ that defines the

unitary evolution of a closed quantum system is then adapted to include a bath dissipator, \mathcal{D}_B , which describes the interaction of the system with the hot and cold baths and introduces non-unitary behaviour into the system dynamics. The resulting well-established GKLS equation has the form [20]

$$\dot{\rho}(t) = -i[H(t), \rho(t)] + \mathcal{D}_B(\rho(t)) \quad (4)$$

with

$$\mathcal{D}_B(\rho(t)) = \sum_{n=+, -, 0} \gamma_n (P_n \rho(t) P_n^\dagger - 1/2 \{P_n^\dagger P_n, \rho(t)\}), \quad (5)$$

where $P_{+,-,0}$ are jump operators ($P_+ = |e\rangle\langle g|$, $P_- = |g\rangle\langle e|$, and $P_0 = |e\rangle\langle e| - |g\rangle\langle g|$) and γ_n are the corresponding Lindblad rates. The rates scale with the bath spectral density, $J(\omega)$, and the occupation number $N(\Omega) = 1/(e^{\Omega\beta} - 1)$ where β is the inverse temperature of the bath: $\gamma_+ = J(\omega)N(\Omega)2\pi \cos^2 \theta$, $\gamma_- = J(\omega)(1 + N(\Omega))2\pi \cos^2 \theta$ and $\gamma_0 = 2\pi(\alpha/\beta) \sin^2 \theta$ (α is the system-bath coupling strength). The spectral density describes the distribution of frequencies at which the system interacts with its environment and is chosen here to be Ohmic, $J(\omega) = \alpha\omega e^{-\omega/\omega_C}$ (ω_C is the cut-off frequency).

To summarise, the system is weakly-coupled to a heat bath on the isochores, but not driven. Conversely, on the isentropes, the system is treated in isolation from the thermal environments but the energy splitting is driven using $\Omega_z(t)$.

C. Noisy Quantum Dynamics

Control noise during the cycle is modelled as a Gaussian White Noise (GWN) process, $\xi_i(t)$, with the following properties [21]: (i) noise values obey a Gaussian distribution centred on zero, $\mathbb{E}[\xi_i(t)] = 0$; (ii) the noise is delta-correlated such that there are no correlations between different noise sources nor with the same source at different times, $\mathbb{E}[\xi_i(t)\xi_j(s)] = \lambda \mathcal{X}_{ij}(t-s)$ where λ characterises the noise strength and $\mathcal{X}_{ij}(t-s) = \delta_{ij}\delta(t-s)$ defines the two-time correlations; (iii) there is no initial correlation, $\mathbb{E}[\xi_i(0)\rho(0)] = 0$. Here, $\mathbb{E}[\dots]$ represents an average over noise-realisations.

Noise is implemented such that it scales with the amplitude of the associated control field:

$$H_\xi(t) = \sum_j \frac{1}{2} \xi_j(t) \Omega_j(t) \sigma_j. \quad (6)$$

The noisy system Hamiltonian is the sum of $H_S(t)$ from Equation (1) and $H_\xi(t)$, $H_{S,\xi}(t) = H_S(t) + H_\xi(t)$. From this and the properties of GWN, (i)-(iii), the noise-averaged dynamics governed by the dissipator $\mathcal{D}_\xi(\mathbb{E}[\rho(t)])$ can be derived (see Appendix A) utilising Novikov's theorem [22] and following the approach in

[23], arriving at:

$$\mathcal{D}_\xi(\mathbb{E}[\rho(t)]) = - \sum_j \frac{\Omega_j(t)^2}{4} \lambda [\sigma_j, [\sigma_j, \mathbb{E}[\rho(t)]]]. \quad (7)$$

The general state evolution equation for the cycle includes both unitary evolution, and additive contributions from noisy controls and weak coupling to a heat bath (hot or cold),

$$\mathbb{E}[\dot{\rho}(t)] = -i [H_S(t), \mathbb{E}[\rho(t)]] + \mathcal{D}_B(\mathbb{E}[\rho(t)]) + \mathcal{D}_\xi(\mathbb{E}[\rho(t)]). \quad (8)$$

More specifically, $\mathcal{D}_B(\mathbb{E}[\rho(t)])$ is not present on isentropes and $H_S(t)$ is time-independent on isochores. Thus, whilst $\mathcal{D}_\xi(\mathbb{E}[\rho(t)])$ is present on all strokes, it is only time-dependent on the isentropes, where $\Omega_j(t)$ varies with time.

D. The Limit Cycle

The focus of this work is on finite-time cycles. Therefore, it would not be appropriate to assume full thermalisation on the isochores, nor adiabatic dynamics on the isentropes. Having been prepared in any input state, after N repetitions of the cycle, the system reaches its limit cycle where the state at a given vertex, m , of consecutive cycles is the same, $\rho_N^m = \rho_{N-1}^m$. The existence of a limit cycle state for a given set-up can be proved by defining the total cycle propagator, \mathcal{V}_{cyc} , and finding the state, ρ_{lim} , on which there is no net effect (the eigenvector of \mathcal{V}_{cyc} with eigenvalue of 1), in vectorised form $\mathcal{V}_{cyc} |\rho_{lim}\rangle\rangle = |\rho_{lim}\rangle\rangle$ [24]. All engines considered here have a unique (noise-averaged) limit cycle state, which has been confirmed by examination of the transient dynamics approaching the limit cycle from initially thermal and collapsed states. All results quoted are of engines operating in their finite-time limit cycles.

III. DEFINING WORK AND HEAT

In order to evaluate the thermodynamic performance of the Otto engine, the quantities of heat and work (currents) are central, from which, for example, we can define efficiency. Macroscopic distinctions between the two quantities are uncontroversial - heat is the exchange of thermal energy, and work the exchange of mechanical energy.

Looking at a quantum system weakly coupled to a thermal bath and driven with noiseless controls, there is also a widely accepted distinction between heat and work. As such, a first law can be formulated for each stroke within the noiseless Otto engine. For stroke j , ran from time t_i

to t_f , the total change in energy expectation is given by

$$\begin{aligned} \langle E_j \rangle &= \langle W_j \rangle + \langle Q_j \rangle \\ &= \int_{t_i}^{t_f} \text{Tr}[\dot{H}_j(t)\rho_j(t)]dt + \int_{t_i}^{t_f} \text{Tr}[H_j(t)\dot{\rho}_j(t)]dt, \end{aligned} \quad (9)$$

where W_j and Q_j represent the work done and the heat transferred to the system and can be associated with their respective terms in the second line, and $\rho_j(t)$ represents the system density matrix across stroke j . Since the trace of a (finite-dimensional) commutator is zero due to the cyclic property of the trace and the evolution of the noiseless system across isentropes is given by the von Neumann equation, the energy expectation on the isentropes is solely due to work exchanged with the system. Conversely, since the Hamiltonian is constant across the isochores, changes in energy expectation are entirely due to \mathcal{D}_B and thus attributed to heat transfer on these strokes. Thus, this distinction assigns unitary changes in energy due to the time-dependent Hamiltonian as work, and non-unitary energy changes encoded by \mathcal{D}_B as heat.

Difficulties arise when dividing noise-induced energetics into heat and work. Noise, when considering individual trajectories, introduces an extra source of time dependence into the system Hamiltonian and thus, according to Equation 9, its effects could be considered as work contributions. Conversely, noisy effects could also be interpreted as a heat cost since the noise-averaged dissipator, \mathcal{D}_ξ , from Equation 7 gives rise to non-unitary evolution.

Here, we adopt a division of noise-induced energy changes into heat and work based on: (a) the distinction between heat and work for an equivalent noiseless process and (b) the naivety of the observer in considering their system as noise-free. Take, for example, a closed quantum stroke where the system is being driven. In the absence of noise, we expect any observed changes in system energy to be work, with no heat contribution. We extrapolate this to noisy controls, whereby the observer still considers any measured energy change along such a stroke as work, even though there is now noise-induced irreversibility and non-unitarity (not commonly associated with work). Conversely, if an open quantum system is held by a constant and noiseless Hamiltonian, any measured energy changes are attributed to heat. If the constant control is now affected by noise, the change in energy over that stroke is still considered to be heat, even though energy contributions from the noise are not necessarily sourced from, or dissipated by, a thermal bath. Thus, in the noisy Otto engine, we consider any energy changes along isentropes to be a form of work, and any energy changes along isochores as heat. We recognise limitations of this approach when generalising, for example, to situations where the system is intentionally driven and in contact with a bath but, for the purposes of this paper, this classification will suffice.

IV. ENHANCEMENT TECHNIQUES

In thermodynamics, adiabaticity refers to the minimisation of dissipation and, hence, entropy production. Adiabatic processes have maximal efficiency; for engines, this is equal to the Carnot efficiency, $\eta_C = 1 - T_C/T_H$ [1]. Ordinarily this optimal efficiency can only be achieved in the infinite time-limit, where power output is zero. Thus, there is a trade-off between power and efficiency. Under the assumptions of perfect thermalisation on isochores and noiseless adiabatic driving on isentropes, the maximum work output and heat of the Otto engine can be found by taking the energy expectation value of the system at each vertex over one cycle, yielding

$$\begin{aligned} W_{max} &= \frac{(\Omega_H - \Omega_C)}{2} \left[\tanh\left(\frac{\beta_C \Omega_C}{2}\right) - \tanh\left(\frac{\beta_H \Omega_H}{2}\right) \right], \\ Q_{H,max} &= \frac{\Omega_H}{2} \left[\tanh\left(\frac{\beta_C \Omega_C}{2}\right) - \tanh\left(\frac{\beta_H \Omega_H}{2}\right) \right]. \end{aligned} \quad (10)$$

Thus, the optimal Otto efficiency in quantum engines can be calculated as $\eta_O = 1 - \Omega_C/\Omega_H$. This is equivalent to η_C in the instance where $\Omega_C/\Omega_H = T_C/T_H$, in which case there is zero work output. Thus, a trade-off between efficiency and power exists for noiseless quantum engines with respect to the driving parameter $\Omega(t)$. Further, as in the classical case, a similar trade-off may be expected with respect to the choice of τ , the cycle operation time: as $\tau \rightarrow \infty$, power output approaches zero and efficiency becomes maximal.

When the system is driven over a finite time and the Hamiltonian is not two-time-commuting, off-diagonal non-adiabatic correction terms appear in the eigenbasis of the system Hamiltonian evolution:

$$\begin{aligned} \dot{\rho}'(t) &= \frac{d}{dt} (R^\dagger(t)\rho(t)R(t)) \\ &= -i [H'_S(t), \rho'(t)] + i \left[\frac{\dot{\theta}(t)\sigma_y}{2}, \rho'(t) \right]. \end{aligned} \quad (12)$$

The dynamics induced by such terms generates coherences in the system energy eigenbasis and has an associated energetic cost, coined quantum friction.

Methods of quantum enhancement can, in theory, be implemented to counteract the accumulation of quantum friction in the system and thus to recover adiabatic behaviour in finite operation times. One approach is to apply a *shortcut to adiabaticity* (STA) [25]. One widely applicable STA is counterdiabatic driving which involves applying an auxiliary field to the system that directly cancels the non-adiabatic correction terms [26]. Here, the Hamiltonian for counterdiabatic driving [27] on the engine isentropes is $H_{STA}(t) = \frac{1}{2}\Omega_y(t)\sigma_y$, where $\Omega_y(t) = \dot{\theta}(t) = -\frac{\Omega_x\dot{\Omega}_z(t)}{\Omega_x^2 + \Omega_z(t)^2}$. When noise is considered, the externally-driven STA field will also be subject to

amplitude noise in the same fashion as other controls (Equation 6).

Another approach to avoid quantum friction effects is *quantum lubrication* (QL) [28], where a pure-dephasing (noisy) field is applied to the system. A noise source is pure-dephasing with respect to an observable X if its dissipator (derived from Equation 7) acts only and negatively on the coherences (off-diagonals) of the system density matrix in the eigenbasis of X . This is achieved for the energy observable $H_S(t)$ when the noisy lubricating field is proportional to $\sigma'_z(t)$ in the $H_S(t)$ eigenbasis ($\sigma'_z(t) = (\Omega_z(t)\sigma_z + \Omega_x\sigma_x)/\Omega(t)$ in the unrotated basis). An applied field of $H'_{QL}(t) = \xi_{QL}(t)\sigma'_z(t)$, where $\xi_{QL}(t)$ is a GWN source with controllable noise strength $\lambda_{QL}(t)$, also ensures that the original Hamiltonian (Equation 1) is returned after noise-averaging. Here, we take λ_{QL} to be constant. The pure-dephasing dissipator then acts as

$$\begin{aligned} \mathcal{D}_{QL}(\mathbb{E}[\rho'(t)]) &= -\lambda_{QL}[\sigma'_z(t), [\sigma'_z(t), \mathbb{E}[\rho'(t)]]] \\ &= -4\lambda_{QL} \begin{pmatrix} 0 & \rho'_{01}(t) \\ \rho'_{10}(t) & 0 \end{pmatrix}, \end{aligned} \quad (13)$$

where $\rho'_{ij}(t)$ is the entry on the i^{th} row and j^{th} column of the system state, $\rho(t)$, expressed in the (noise-averaged) energy eigenbasis.

Thus, Equation 8 can be adapted for enhanced isentropes either by QL,

$$\begin{aligned} \mathbb{E}[\dot{\rho}(t)] &= -i[H_S(t), \mathbb{E}[\rho(t)]] + \mathcal{D}_\xi(\mathbb{E}[\rho(t)]) \\ &\quad + \mathcal{D}_{QL}(\mathbb{E}[\rho(t)]), \end{aligned} \quad (14)$$

or by an STA,

$$\begin{aligned} \mathbb{E}[\dot{\rho}(t)] &= -i[H_S(t) + H_{STA}(t), \mathbb{E}[\rho(t)]] \\ &\quad + \mathcal{D}_\xi(\mathbb{E}[\rho(t)]), \end{aligned} \quad (15)$$

where in the latter case $\mathcal{D}_\xi(\mathbb{E}[\rho(t)])$ is adapted to include an extra noise term proportional to $H_{STA}(t)$.

V. AVERAGE PERFORMANCE

We are now in a position to assess the average performance of the Otto engine model described in the previous sections. In this section, we will compare an unenhanced, nonadiabatic (NA) engine with its corresponding STA and QL counterparts, where results are generated by numerically solving the dynamics along successive strokes.

Looking at the NA engine operation (Figure 2, dashed lines), control noise is seen to routinely worsen engine performance. In the noiseless case (orange), power is maximised at short cycle times, τ , whilst efficiency is maximised as $\tau \rightarrow \infty$, thus exhibiting the classical trade-off between power and efficiency. With noise, the NA engine has maximal power and efficiency under a pseudo-bang-bang control strategy (near instantaneous driving).

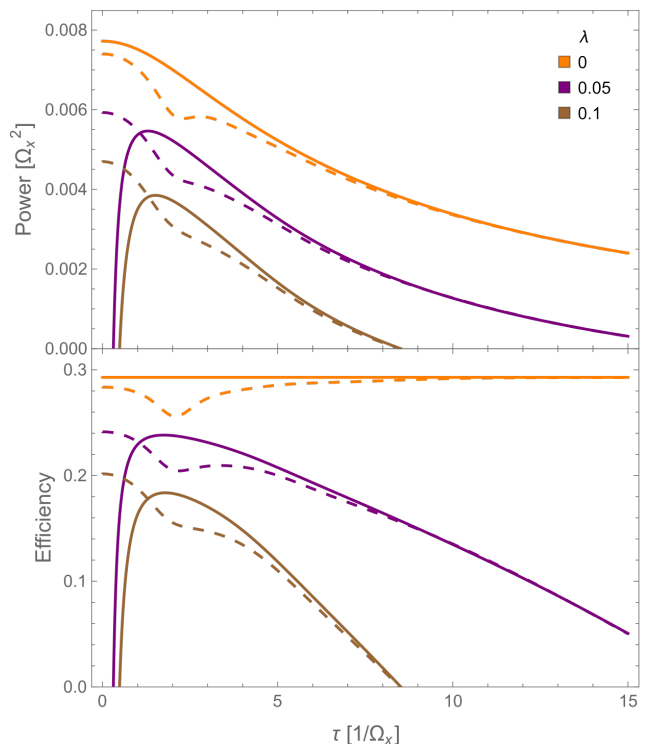


Figure 2. The power (top) and efficiency (bottom) of the engine in the presence of three different levels of noise, λ , across different cycle times, τ , given in units of intrinsic system energy scales, Ω_x . In all plots, the solid lines represent an engine with an STA and the dashed lines without. The environment parameters are: $\alpha = 0.01$, $\Omega_C = 100$, $T_C = T_H/5 = 10\Omega_x$.

When an STA is applied (solid lines), the efficiency is maximised at the Otto efficiency in the absence of control noise, where $\eta(\tau) = \eta_O \forall \tau$. When control noise is present, power and efficiency peak at similar, but not exactly equivalent, finite cycle times. STAs are found to improve engine performance with diminishing returns at larger cycle times, demonstrating the legitimacy of STAs in recapturing adiabatic dynamics. Notably, with noisy controls the power and efficiency of engines with STAs are degraded at small τ below a critical operation time, τ_{STA} . More generally, counterdiabatic driving is expected to be ineffective for fast driving with amplitude-noise. This is because $H_{STA}(t)$ will act to counteract non-adiabatic correction terms (proportional to $\dot{\Omega}_z(t)$); meaning the faster the controls are swept, the greater the magnitude of $H_{STA}(t)$. Therefore, since amplitude noise scales with the magnitude of the control field, the STA field is more affected by noise when the system is driven quickly. Looking at an individual trajectory this means that $H_{STA}(t)$ is highly inexact and fails to cancel the non-adiabatic correction terms. When looking at the noise-averaged dynamics, this corresponds to a large $\mathcal{D}_\xi(\mathbb{E}[\rho(t)])$ associated with the STA field. Since the intended applications for STAs are usually at shorter timescales, the existence of τ_{STA} is noteworthy. Never-

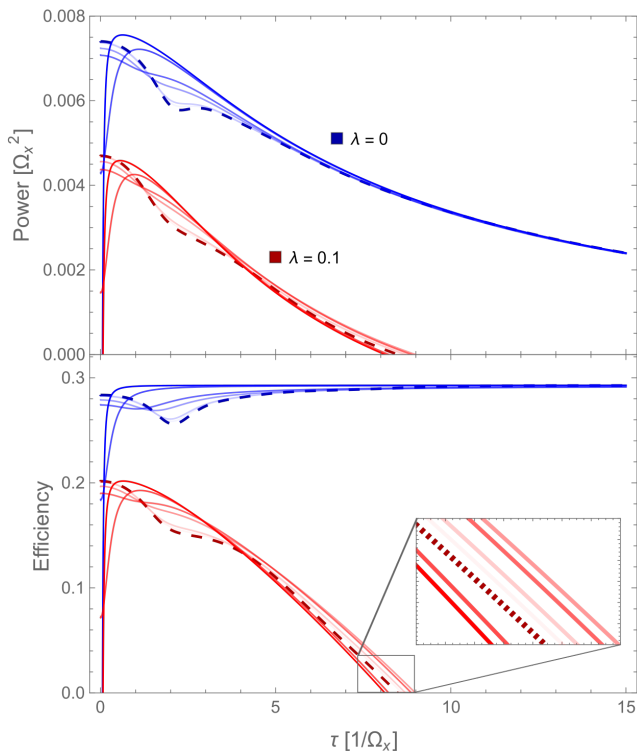


Figure 3. The power (top) and efficiency (bottom) of the quantum Otto cycle with different strengths of lubricating noise, λ_{QL} (solid), with (red) and without (blue) control noise, λ . This is shown in comparison to NA performance (dashed) across different cycle times, τ , given in units of intrinsic system energy scales, Ω_x . $\lambda_{QL} = \{0.05, 0.1, 0.5, 1, 10, 100\}$ increasing with degree of colour saturation. The environment parameters are: $\alpha = 0.01$, $\Omega_C = 100$, $T_C = T_H/5 = 10\Omega_x$.

theless, counterdiabatic driving is predicted to improve efficiency and power at operation times larger than τ_{STA} . The time domain where STAs are effective is broadened as τ_{STA} is reduced, which can be achieved by lowering noise levels, λ , or increasing $\Omega(t)/\Omega_x$. For experimental realisations with energies of the order of 1 GHz, effective timescales for STA use are $\tau_{STA} \approx 1/\Omega_x = 1$ ns.

Turning to Figure 3, in the noiseless case QL is successful in recovering adiabatic dynamics at finite time when the dephasing noise is strong (darker solid blue lines). With weak dephasing noise (lighter blue), performance improves but remains sub-optimal, except at very short times when retaining coherence is advantageous [17] (see also the next section). When control noise is present, unlike STA engines, those with QL can retain positive performance even at very small τ (weak QL), and can also have a larger maximum power production than STA engines (strong QL). However, at larger τ , the QL engine behaves non-trivially. Depending on λ_{QL} , QL can worsen engine performance or improve it beyond adiabatic predictions. This is likely due to the fact that, in the presence of noise, the instantaneous eigenbasis of the Hamiltonian is fluctuating. Therefore, the dephasing

noise, which is applied diagonally in the noise-averaged eigenbasis, no longer commutes with the system Hamiltonian. Equivalently, in the noise-averaged formalism, $\mathcal{D}_{QL}(\mathbb{E}[\rho'(t)])$ interferes with the action of $\mathcal{D}_\xi(\mathbb{E}[\rho'(t)])$ by destroying its off-diagonal contribution to $\dot{\rho}'(t)$, as well as non-adiabatic Hamiltonian contributions. Thus the dephasing field can give rise to non-intuitive energetic contributions; e.g. at large τ there is an optimal value for λ_{QL} (≈ 4) up to which performance improves above that of the NA engine and beyond which performance reduces.

Despite its detrimental behaviour at both very small and large τ , in the remaining analysis and comparison between approaches we continue with strong QL ($\lambda_{QL} = 100$) due its advantages for other τ values.

VI. PERFORMANCE FLUCTUATIONS

A. 4-Point Measurement Scheme

As seen, the classical trade-off between power and efficiency is not present in an idealised quantum regime (noiseless conditions and with the use of an STA). However, there is a third measure of performance which suffers in the quantum regime, as opposed to macroscopic engines: *constancy* [29]. The variance in power, a measure of constancy, can be calculated by implementing a 4-point measurement scheme (4PMS) on the vertices of the cycle to generate a power probability distribution, in a similar manner to Ref. [30].

The probability distribution of the power, $\mathcal{P}(P)$, can be derived from the probabilities of energy changes around the cycle,

$$\mathcal{P}(W_{01}, Q_H, W_{23}) = \mathcal{P}(W_{23}|Q_H)\mathcal{P}(Q_H|W_{01})\mathcal{P}(W_{01}), \quad (16)$$

where, as per Figure 1: $\mathcal{P}(W_{01})$ is the probability of measuring work W_{01} on the compression stroke of the cycle; $\mathcal{P}(Q_H|W_{01})$ represents the conditional probability of measuring heat Q_H given that, on the previous stroke, a work of W_{01} was measured; and $\mathcal{P}(W_{23}|Q_H)$ is defined similarly. If state m is measured at the end of the previous stroke, $\mathcal{P}(Q_H|W_{01}) = \sum_s \delta[Q_H - (\Omega_s - \Omega_m)]p_{m \rightarrow s}^{\tau_{12}}$. Here, $p_{m \rightarrow s}^{\tau_{12}}$ denotes the transition probability from energy eigenstates $|m\rangle$ to $|s\rangle$ over the time τ_{12} corresponding to the hot isochore, and Ω_m denotes the eigenvalue of $|m\rangle$ which, according to Equation 2, is 0 if $|m\rangle$ is the ground state or $\Omega(t)$ if $|m\rangle$ is excited.

Stitching these conditional probabilities together we can expand Equation 16 to obtain

$$\begin{aligned} \mathcal{P}(W_{01}, Q_H, W_{23}) = \sum_{n,m,s,v} & \delta[W_{23} - (\Omega_s - \Omega_v)] \\ & \delta[Q_H - (\Omega_s - \Omega_m)] \\ & \delta[W_{01} - (\Omega_n - \Omega_m)] \\ & p_n^0 p_{n \rightarrow m}^{\tau_{01}} p_{m \rightarrow s}^{\tau_{12}} p_{s \rightarrow v}^{\tau_{23}}. \end{aligned} \quad (17)$$

The above equation sums over all initial states, n , and their possible trajectories across the remaining 3 measurements around the cycle. The initial measurement probabilities p_n^0 are taken directly from the populations of the density matrix in the limit cycle at the beginning of the compression isentrope.

We can select the probability distribution of the power by integrating over all trajectories around the cycle and imposing a definition of the power using a Dirac delta function,

$$\begin{aligned} \mathcal{P}(P) &= \int_{-\infty}^{\infty} \mathcal{P}(W_{01}, Q_{12}, W_{23}) \delta \left[P - \frac{W_{01} + W_{23}}{\tau} \right] \\ &\quad dW_{01} dQ_{12} dW_{23} \\ &= \sum_{n,m,s,v} \delta \left[P - \frac{\Omega_n - \Omega_m + \Omega_s - \Omega_v}{\tau} \right] \\ &\quad p_n^0 p_{n \rightarrow m}^{\tau_{01}} p_{m \rightarrow s}^{\tau_{12}} p_{s \rightarrow v}^{\tau_{23}}. \end{aligned} \quad (18)$$

The moments of the power distribution can then be found by integrating over all measurement trajectories,

$$\langle P^\alpha \rangle = \int_{-\infty}^{\infty} \mathcal{P}(P) P^\alpha dP, \quad (19)$$

and used to define fluctuation measures like the variance.

The transition probabilities, $p_{i \rightarrow j}^{\tau_k}$, have the general form $|\langle j(\tau_k) | V(\tau_k, 0) | i(0) \rangle|^2$ where $V(t, 0)$ represents the time evolution operator along the stroke. Equivalently, in Fock space, stroke propagators describe the evolution of the system over individual strokes such that $\mathcal{V}(\tau_k, 0) |\rho_0\rangle\rangle = |\rho_{\tau_k}\rangle\rangle$, where $\mathcal{V}(\tau_k, 0)$ is calculated from the associated Liouvillian superoperator for that stroke; $\dot{\mathcal{V}}(t, 0) = \mathcal{L}(t) \mathcal{V}(t, 0)$ with $|\dot{\rho}_t\rangle\rangle = \mathcal{L}(t) |\rho_t\rangle\rangle$. Thus, $p_{i \rightarrow j}^{\tau_k}$ can be more usefully represented using stroke propagators in Fock space,

$$\begin{aligned} p_{i \rightarrow j}^{\tau_k} &= \langle j(\tau_k) | V(\tau_k, 0) | i(0) \rangle \langle i(0) | V^\dagger(\tau_k, 0) | j(\tau_k) \rangle \\ &= \langle j(\tau_k) | V(\tau_k, 0) \rho_0^i V^\dagger(\tau_k, 0) | j(\tau_k) \rangle \\ &= \left(\langle j(\tau_k) | \otimes | j(\tau_k) \rangle^T \right) \mathcal{V}(\tau_k, 0) |\rho_0^i\rangle\rangle. \end{aligned} \quad (20)$$

Taking the state at the beginning of the stroke to be collapsed, $|i(0)\rangle\langle i(0)|$, and then operating on this state with the stroke propagator over time τ_k , the transition probability to the state of interest $|j(\tau_k)\rangle$ is selected using $\langle j(\tau_k) | \dots | j(\tau_k) \rangle$.

When noise is present on the control, the x^{th} moment of power (also applicable to other thermodynamic observables) is given by:

$$\begin{aligned} \mathbb{E}[\langle P^x \rangle] &= \mathbb{E} \left[\int_{-\infty}^{\infty} \mathcal{P}(P) P^x dP \right] \\ &= \sum_{n,m,s,v} \left[\frac{\Omega_n - \Omega_m + \Omega_s - \Omega_v}{\tau} \right]^x \\ &\quad \mathbb{E} [p_n^0] \mathbb{E} [p_{n \rightarrow m}^{\tau_1}] \mathbb{E} [p_{m \rightarrow s}^{\tau_2}] \mathbb{E} [p_{s \rightarrow v}^{\tau_3}]. \end{aligned} \quad (21)$$

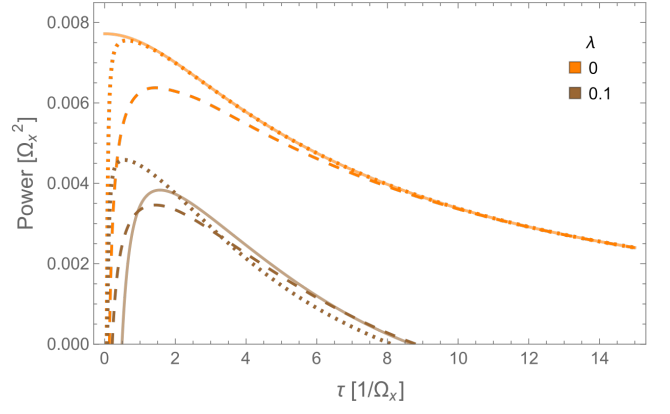


Figure 4. The power of the engine calculated using a 4PMS, in the presence of two different levels of control noise, λ , across different cycle times, τ , given in units of intrinsic system energy scales, Ω_x . Solid lines represent a STA engine, dotted lines a QL engine (with $\lambda_{QL} = 100$), and dashed lines an NA engine. The environment parameters are: $\alpha = 0.01$, $\Omega_C = 100$, $T_C = T_H/5 = 10\Omega_x$.

In reaching the second equality, we have made two assumptions. First, we note that the energy measurements themselves are independent of the applied control fields and are taken to be noise-free. Therefore, measurement returns energy eigenvalues, Ω_i , in the (noise-averaged) basis in which we are performing our measurements. This is justified by a fundamental postulate of quantum mechanics: that the measurement of an observable by an operator, \hat{A} , will always return an eigenvalue a of that operator, where $\hat{A}|\psi\rangle = a|\psi\rangle$. Second, as a continuation of the Markov property of white noise, where noise is uncorrelated with itself at different times, the noise-averaging acts independently on the transition probabilities. Thus, Equation 20 accommodates noisy dynamics by the replacement $\mathcal{V}(\tau_k, 0) \rightarrow \mathbb{E}[\mathcal{V}(\tau_k, 0)]$.

B. Average Performance with 4PMS

The average performance calculated using the 4PMS may be expected to generate significantly different results from that given in Figure 2. This is because coherence is destroyed as the state is collapsed by projective measurements on each vertex of the 4PMS. On the other hand, when using the energy expectation at the vertices, no such disruption occurs. Indeed, in Figure 4 we find that results differ between the approaches, most significantly for the NA engine ran quickly ($\tau < 1$). This follows from the fact that under these conditions coherence generation is largest (enhancement and slower driving reduce coherence). Interestingly, the NA engine's performance degrades when calculated using the 4PMS which suggests that, at short operation times, coherence generation can contribute positively to performance. Figure 4 also shows that QL is potentially the most effective enhancement approach when the cycle is measured according to the

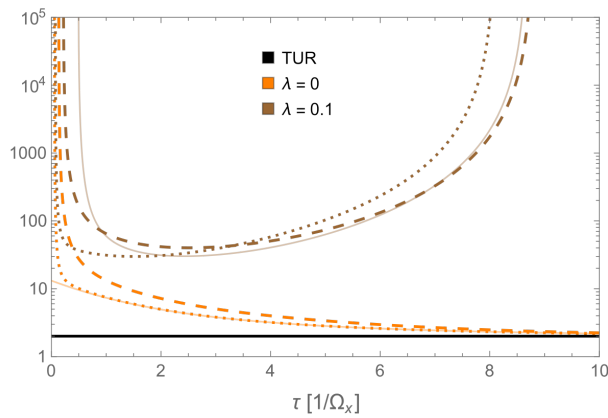


Figure 5. The power fluctuations, $\frac{\Delta_P^2}{P_\tau^2} \dot{\Sigma}$, and TUR bound (equal to 2 in Equation 22), at different noise levels for a single cycle of the engine across different cycle times, τ , given in units of intrinsic system energy scales, Ω_x . Coloured solid lines represent fluctuations of an STA engine, the dotted lines of a QL engine (with $\lambda_{QL} = 100$), and dashed lines of an NA engine. The environment parameters are: $\alpha = 0.01$, $\Omega_C = 100$, $T_C = T_H/5 = 10\Omega_x$

4PMS. Lastly, as τ increases, results for average performance found using energy expectation values and using the 4PMS coalesce (not plotted).

These features are in agreement with literature [17], whereby at short cycle times and at certain system-bath coupling strengths, it is suggested that a quantum heat engine outperforms a classical stochastic model of a heat engine (without coherence), with the performances of the two engines becoming equal at larger cycle times when thermalisation with the bath is reached and the system fully decoheres.

The Otto engine has recently been realised experimentally in [10] and [11], utilising projective measurements and nuclear magnetic resonance techniques on C-13 nuclei. The generated results agree qualitatively with the results of this paper. Specifically, positive work (power) output is observed only at finite cycle times ($\tau > \tau_{\min}$). Such features could potentially originate, according to this theoretical model, due to the destruction of coherence from projective measurements (as seen in Figure 4).

C. Thermodynamic Uncertainty Relation

Thermodynamic uncertainty relations (TURs) are inequalities that relate fluctuations of currents to the average entropy production, becoming increasingly relevant when driving further from equilibrium and when smaller systems are considered [31, 32]. With their conception in the field of statistical thermodynamics, they also apply to and have found underpinning in the quantum regime [33]. Here, a bound on power variance originating from a TUR is used as a consistency check for the variance

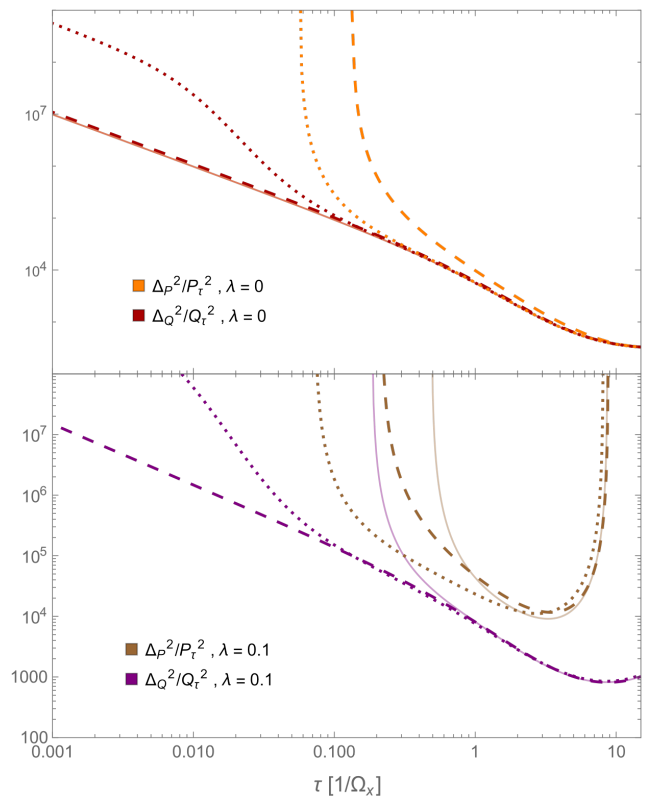


Figure 6. The power and heat Fano factors under noiseless (top) and noisy (bottom) conditions, for a single cycle of the engine across different cycle times, τ , given in units of intrinsic system energy scales, Ω_x . Solid lines represent fluctuations of an STA engine, the dotted lines of a QL engine (with $\lambda_{QL} = 100$), and dashed lines of an NA engine. All parameter values are the same as Figure 5

calculations using the 4PMS in Equation 19, and also to observe the tightness of the bound for different scenarios.

A relevant TUR relates the noise- and time-averaged variance in power (a work current), $\Delta_P^2/\tau = (\mathbb{E}[\langle P^2 \rangle] - \mathbb{E}[\langle P \rangle]^2)$, to the noise-averaged power, $P_\tau = \mathbb{E}[\langle P \rangle]$, and the entropy production rate, $\dot{\Sigma}$, over a cycle:

$$\frac{\Delta_P^2}{P_\tau^2} \geq \frac{2}{\dot{\Sigma}}. \quad (22)$$

This TUR is derived in accordance with Refs. [34] and [35], valid for time-symmetric driving and unital dynamics [36] on the isentropic strokes, as is the case here. It is worth noting that Equation 22 is also consistent with a bound derived for more general periodic quantum heat engines in the slow-driving limit [37], where the attained corrections for time-asymmetric driving and generation of quantum friction vanish for the model under review. Furthermore, Equation 22 coincides with the form of TUR applicable to steady-state heat engines [29].

The form of Equation 22 indicates the usefulness of the Fano factor [38] as a measure of fluctuations, defined here

as $F(P) = \Delta_P^2/P_\tau^2$. We see that smaller fluctuations are permitted by increasing the dissipation $\dot{\Sigma}$; for instance, if we desire to reduce Δ_P^2 , then we must decrease the average power or increase entropy production. For a cyclic engine, $\dot{\Sigma}$ is given by the sum of entropy fluxes from contact with heat baths and the change in von Neumann entropy, ΔS_{VN} , per cycle:

$$\dot{\Sigma} = \frac{1}{\tau} \Delta S_{VN} - \sum_{i \in H, C} \beta_i \dot{Q}_i, \quad (23)$$

where \dot{Q}_i is the heat current into bath i . For an engine operating in its limit cycle, $\Delta S_{VN} = 0$, and $\dot{\Sigma}$ can be expressed using only the power, inverse temperature of the cold bath, efficiency, and Carnot efficiency of the cycle [32]. With this, we can reformulate the above TUR in terms of efficiency, power and power variance in order to explicitly show the existence of a trade-off between the three quantities:

$$\frac{\Delta_P^2}{P_\tau^2} \geq \frac{2P_\tau \eta}{\beta_C (\eta_C - \eta)}, \quad (24)$$

where all quantities have been defined previously.

The existence of a trade-off between average performance and constancy is consistent with Figures 5 and 6, where the measured fluctuations increase at cycle times when average performance is optimal ($\tau \leq 1.5$ from Figure 4). Furthermore, in figure 5 the noiseless and noise-averaged variances are shown to always be greater than the TUR bound as required. The measured power fluctuations for noisy controls (brown) increase sharply at $\tau \approx 8$ corresponding to the point where the engine ceases to produce a power output (see Figure 2). At $\tau \gtrsim 8$, the cycle functions as an inverted heat pump, consuming work and accelerating the transport of heat from the hot to the cold bath. The performance fluctuations are only displayed for operation times when the cycle is operating successfully as a heat engine.

The variances of STA and NA engines become equal at larger times ($\tau \approx 10$), illustrated by the coalescence of dashed and solid lines of the same colour in Figures 5 and 6. This is in agreement with investigations [39] into the fluctuations of STA protocols without control noise. It was predicted that, although greater fluctuations occur at intermediate times during STA control strokes, at the end of the STA stroke, as calculated here, the variance should be the same as a truly adiabatic stroke without a shortcut. Conversely, most apparent in Figure 5, the power fluctuations of the QL engine differ from the NA engine for most cycle times. This follows from the deviating average performance between the QL and NA engines (Figure 4).

Another feature to note is that the TUR bound is saturated in the noiseless set-up faster than when control noise is present (this occurs at $\tau \gg 15$, not shown); in other words, the TUR bound for noisy engines is not as tight. This indicates, rather straightforwardly, that there are unnecessary fluctuations when noise exists on

the controls. Lastly, for all engines, the calculated fluctuations in performance are significant with respect to the average performance, with $F(P)$ consistently greater than 1.

In Figure 6, the Fano factors of Q_H and P are displayed across different cycle times. As predicted in Refs. [34], the relative fluctuation of power is shown to always be greater than or equal to the relative fluctuation of input heat, $F(P) \geq F(Q_H)$, with the equality reached in the adiabatic limit. In addition, Figure 6 highlights the short-time fluctuations of output power (represented by the orange and brown lines): with noiseless controls, an STA gives rise to the lowest fluctuations; and, with noisy controls, QL is the most reliable approach, whilst an STA increases the fluctuations beyond that which is achieved non-adiabatically.

VII. CONCLUSION

A model of a quantum Otto engine can overcome a classical trade-off between power output and working efficiency with respect to cycle operation time, when controls are noise-free. However, fluctuations in performance scale with improved average performance, consistent with bounds from the TUR. The destruction of coherence within the engine cycle via projective measurements was seen to worsen performance, especially in NA engines, aiding the conception that coherence can benefit work extraction.

An STA was shown to improve average engine performance at intermediate cycle times but was found to act detrimentally at short cycle times, due to the scaling of noise in the auxiliary field with rate of driving $\dot{\Omega}_z(t)$. Slower engines become quasi-adiabatic and therefore the presence of an STA ceases to be beneficial. QL recovers adiabatic dynamics in the absence of control noise but fails to commute with the fluctuating system Hamiltonian when control noise is introduced and thus contributes non-trivial energetics dependent on the strength of the lubricating noise. Thus, whilst engine performance is consistently improved by quantum enhancement techniques if auxiliary controls are noiseless, this is not generally the case for noisy controls.

Further research into the generalisability of these results to other models of noise, working systems, enhancement techniques (such as noise resistant STAs [40]) and quantum devices would be of interest. Additionally, an in-depth investigation into different conceptions of heat and work would be fruitful for future studies on the thermodynamics of noisy quantum control.

Appendix A: Derivation of \mathcal{D}_ξ

This appendix concerns itself with deriving the Lindblad dissipator, \mathcal{D}_ξ , due to noisy controls in the general time-dependent case, as in Equation 7. A reminder that

we are considering GWN with correlations described by

$$\mathcal{X}_{ij}(t-s) = \delta_{ij}\delta(t-s) \quad (\text{A1})$$

with variance λ . The result for \mathcal{D}_ξ is unusual in the sense that the noise strength is time-dependent, scaling with the amplitudes of the driving fields. Thus, we will focus on a closed system with time-dependent driving, an isentrope. (Note that, certainly on isochores where the driving is static, \mathcal{D}_ξ behaves additively with a bath dissipator D_B if the system is also coupled to a thermal reservoir. This result is not proven here but can be achieved by moving into the interaction picture with respect to the noisy dynamics and performing the below treatment of noise-averaging prior to dealing with bath terms).

If $M(\xi)$ is a functional of the real-valued noise, ξ , with $\mathbb{E}[\xi_i(t)\xi_j(s)] = \lambda\mathcal{X}_{ij}(t-s)$, then Novikov's theorem can be written as [22]:

$$\begin{aligned} \mathbb{E}[\xi_\alpha(t)M(\xi)] &= \mathbb{E}[\xi_\alpha(t)]\mathbb{E}[M(\xi)] \\ &+ \int_0^t dt_1 \mathcal{X}_{\alpha\beta}(t-t_1)\mathbb{E}\left[\frac{\delta M(\xi)}{\delta \xi_\beta(t_1)}\right] \end{aligned} \quad (\text{A2})$$

where $\frac{\delta M(\xi)}{\delta \xi_\beta(t_1)}$ represents the functional derivative of $M(\xi)$ with respect to the noise source ξ_β at time t_1 . We adopt from here forward the convention of implicit summation over repeated indices.

The trajectory-dependent evolution of the state across a noisy isentrope is given by $\rho(t)$, with dynamics

$$\frac{d}{dt}\rho(t) = -i[H_S(t) + H_\xi(t), \rho(t)] \quad (\text{A3})$$

where, as in the main script, we have set $\hbar = 1$. For the time-being we use a condensed notation, defining a new Hermitian operator $K_\alpha(t) = \frac{1}{2}\Omega_\alpha(t)\sigma_\alpha$ such that $H_\xi(t) = \sum_\alpha K_\alpha \xi_\alpha(t)$. Note that any additional Hamiltonian terms representing enhancement techniques can also be divided into their deterministic and stochastic parts, retaining the form of A3. Therefore, although not explicitly treated, results in this section apply equally to enhanced strokes.

Following [41], we recognise that $\rho(t)$ is a functional of ξ_α . Utilising this fact, we can apply A2 as

$$\begin{aligned} \mathbb{E}[H_\xi(t)\rho(t)] &= \mathbb{E}[\xi_\alpha(t)K_\alpha(t)\rho(t)] \\ &= \mathbb{E}[\xi_\alpha(t)]\mathbb{E}[K_\alpha(t)\rho(t)] \\ &+ \int_0^t dt_1 \mathcal{X}_{\alpha\beta}(t-t_1)\mathbb{E}\left[\frac{\delta K_\alpha(t)\rho(t)}{\delta \xi_\beta(t_1)}\right] \\ &= \int_0^t dt_1 \mathcal{X}_{\alpha\beta}(t-t_1)K_\alpha(t)\mathbb{E}\left[\frac{\delta \rho(t)}{\delta \xi_\beta(t_1)}\right]. \end{aligned} \quad (\text{A4})$$

Given the Gaussian nature of ξ_α with zero-mean, the first term from Equation A2 goes to zero here. Further, since $K_\alpha(t)$ is independent of any ξ_α , it can be taken outside

the functional derivative. Similarly,

$$\mathbb{E}[\rho(t)H_\xi(t)] = \int_0^t dt_1 \mathcal{X}_{\alpha\beta}(t-t_1)\mathbb{E}\left[\frac{\delta \rho(t)}{\delta \xi_\beta(t_1)}\right]K_\alpha(t). \quad (\text{A5})$$

From here we follow the approach laid out in [23]. Noise-averaging Equation A3 and substituting in Equations A4 and A5,

$$\begin{aligned} \frac{d}{dt}\mathbb{E}[\rho(t)] &= -i[H_S(t), \mathbb{E}[\rho(t)]] \\ &- i \int_0^t dt_1 \mathcal{X}_{\alpha\beta}(t-t_1) \left[K_\alpha(t), \mathbb{E}\left[\frac{\delta \rho(t)}{\delta \xi_\beta(t_1)}\right] \right]. \end{aligned} \quad (\text{A6})$$

We now focus our efforts on gaining an expression for $\frac{\delta \rho(t)}{\delta \xi_\beta(t_1)}$, as all other quantities in A6 are already known. Starting from the exact solution to A3,

$$\rho(t) = \rho(0) - i \int_0^t ds [H_S(s) + H_\xi(s), \rho(s)], \quad (\text{A7})$$

we take the functional derivative with respect to $\xi_\beta(t_1)$:

$$\begin{aligned} \frac{\delta \rho(t)}{\delta \xi_\beta(t_1)} &= \frac{\delta \rho(0)}{\delta \xi_\beta(t_1)} \\ &- i \int_0^t ds \left[\frac{\delta (H_S(s) + H_\xi(s))}{\delta \xi_\beta(t_1)}, \rho(s) \right] \\ &- i \int_0^t ds \left[H_S(s) + H_\xi(s), \frac{\delta \rho(s)}{\delta \xi_\beta(t_1)} \right] \quad (\text{A8}) \\ &= -i[K_\beta(t_1), \rho(t_1)] \\ &- i \int_{t_1}^t ds \left[H_S(s) + H_\xi(s), \frac{\delta \rho(s)}{\delta \xi_\beta(t_1)} \right] \quad (\text{A9}) \end{aligned}$$

We have taken a few actions in reaching A9: the first term on the right-hand side of A8 is taken to be zero as we assume that the state and the noise are initially uncorrelated; the second term is only non-zero when $\alpha = \beta$ and the integrated time $s = t_1$, and reduces to the first term of A9; the noise is causal on the state and not vice-versa so the state $\rho(t < t_1)$ is not affected by any noise $\xi_\beta(t_1)$.

If we differentiate A9 with respect to time, t , we get

$$\frac{d}{dt} \frac{\delta \rho(t)}{\delta \xi_\beta(t_1)} = -i \left[H_S(t) + H_\xi(t), \frac{\delta \rho(t)}{\delta \xi_\beta(t_1)} \right] \quad (\text{A10})$$

which has exactly the same dynamics as $\rho(t)$ in Equation A3, other than the initial condition is given by $\frac{\delta \rho(t_1)}{\delta \xi_\beta(t_1)} = -i[K_\beta(t_1), \rho(t_1)]$. The time-ordered (denoted by \mathcal{T}) unitary evolution operator for $\rho(t)$, $U(t, t_1) = \mathcal{T} \exp\left(-i \int_{t_1}^t ds H_S(s) + H_\xi(s)\right)$, can then be used to generate a solution for $\frac{\delta \rho(t)}{\delta \xi_\beta(t_1)}$ from time t_1 onwards:

$$\frac{\delta \rho(t)}{\delta \xi_\beta(t_1)} = -iU(t, t_1)[K_\beta(t_1), \rho(t_1)]U^\dagger(t, t_1). \quad (\text{A11})$$

Returning to the evolution of $\mathbb{E}[\rho(t)]$ given by Equation A6, we can substitute in the noise-averaged version of A11 such that

$$\begin{aligned} \frac{d}{dt}\mathbb{E}[\rho(t)] &= -i[H_S(t), \mathbb{E}[\rho(t)] - \int_0^t dt_1 \mathcal{X}_{\alpha\beta}(t-t_1) \\ &\times [K_\alpha(t), \mathbb{E}[U(t, t_1)[K_\beta(t_1), \rho(t_1)]U^\dagger(t, t_1)]]]. \end{aligned} \quad (\text{A12})$$

Reference [23] goes on to resolve the time non-local nature of the above equation and perform perturbative expansions in $H_\xi(t)$. For our case, since we are only

considering white noise, we can now enforce the definition of $\mathcal{X}_{\alpha\beta}(t-t_1) = \delta(t-t_1)$ from A1. The above equation then reduces to

$$\begin{aligned} \frac{d}{dt}\mathbb{E}[\rho(t)] &= -i[H_S(t), \mathbb{E}[\rho(t)] \\ &- [K_\alpha(t), [K_\alpha(t), \mathbb{E}[\rho(t)]]], \end{aligned} \quad (\text{A13})$$

making use of the sifting property of the Dirac delta and the fact that $U(t_1, t_1) = \mathbf{1}$. Thus, summing over the repeated indices and re-substituting $K_\alpha(t) = \frac{1}{2}\Omega_\alpha(t)\sigma_\alpha$, we arrive at Equation 7.

-
- [1] R. Kosloff and Y. Rezek, The quantum harmonic otto cycle, *Entropy* **19**, 136 (2017).
- [2] R. Alicki, The quantum open system as a model of the heat engine, *Journal of Physics A: Mathematical and General* **12**, L103 (1979).
- [3] H. E. Scovil and E. O. Schulz-DuBois, Three-level masers as heat engines, *Physical Review Letters* **2**, 262 (1959).
- [4] T. Feldmann and R. Kosloff, Performance of discrete heat engines and heat pumps in finite time, *Physical Review E* **61**, 4774 (2000).
- [5] Y. Rezek and R. Kosloff, Irreversible performance of a quantum harmonic heat engine, *New Journal of Physics* **8**, 83 (2006).
- [6] M. Born, Va fock beweis des adiabatenatzes z, *Phys* **51**, 165 (1928).
- [7] N. Shiraishi, K. Saito, and H. Tasaki, Universal trade-off relation between power and efficiency for heat engines, *Physical review letters* **117**, 190601 (2016).
- [8] J.-T. Bu, J.-Q. Zhang, G.-Y. Ding, J.-C. Li, J.-W. Zhang, B. Wang, W.-Q. Ding, W.-F. Yuan, L. Chen, i. m. c. K. Özdemir, F. Zhou, H. Jing, and M. Feng, Enhancement of quantum heat engine by encircling a liouvillian exceptional point, *Phys. Rev. Lett.* **130**, 110402 (2023).
- [9] J. Klatzow, J. N. Becker, P. M. Ledingham, C. Weinzetl, K. T. Kaczmarek, D. J. Saunders, J. Nunn, I. A. Walmsley, R. Uzdin, and E. Poem, Experimental demonstration of quantum effects in the operation of microscopic heat engines, *Phys. Rev. Lett.* **122**, 110601 (2019).
- [10] J. P. S. Peterson, T. B. Batalhão, M. Herrera, A. M. Souza, R. S. Sarthour, I. S. Oliveira, and R. M. Serra, Experimental characterization of a spin quantum heat engine, *Phys. Rev. Lett.* **123**, 240601 (2019).
- [11] Y. Xiao, D. Liu, J. He, Y. Ma, Z. Wu, and J. Wang, Quantum otto engine with quantum correlations, *Phys. Rev. A* **108**, 042614 (2023).
- [12] L. M. Cangemi, C. Bhadra, and A. Levy, Quantum engines and refrigerators, *Physics Reports* **1087**, 1 (2024), quantum engines and refrigerators.
- [13] L. Li, H. Li, W. Yu, Y. Hao, L. Li, and J. Zou, Shortcut-to-adiabaticity quantum tripartite otto cycle, *Journal of Physics B: Atomic, Molecular and Optical Physics* **54**, 215501 (2021).
- [14] O. Abah, M. Paternostro, and E. Lutz, Shortcut-to-adiabaticity quantum otto refrigerator, *Phys. Rev. Res.* **2**, 023120 (2020).
- [15] K. Huang, C. Xi, X. Long, H. Liu, Y.-a. Fan, X. Wang, Y. Zheng, Y. Feng, X. Nie, and D. Lu, Experimental realization of self-contained quantum refrigeration, *Phys. Rev. Lett.* **132**, 210403 (2024).
- [16] J. Oppenheim and Z. Weller-Davies, The constraints of post-quantum classical gravity, *Journal of High Energy Physics* **2022**, 1 (2022).
- [17] R. Uzdin, A. Levy, and R. Kosloff, Equivalence of quantum heat machines, and quantum-thermodynamic signatures, *Phys. Rev. X* **5**, 031044 (2015).
- [18] R. Kosloff and A. Levy, Quantum heat engines and refrigerators: Continuous devices, *Annual review of physical chemistry* **65**, 365 (2014).
- [19] P. P. Hofer, M. Perarnau-Llobet, L. D. M. Miranda, G. Haack, R. Silva, J. B. Brask, and N. Brunner, Markovian master equations for quantum thermal machines: local versus global approach, *New Journal of Physics* **19**, 123037 (2017).
- [20] H.-P. Breuer, F. Petruccione, *et al.*, *The theory of open quantum systems* (Oxford University Press on Demand, 2002).
- [21] A. A. Clerk, M. H. Devoret, S. M. Girvin, F. Marquardt, and R. J. Schoelkopf, Introduction to quantum noise, measurement, and amplification, *Rev. Mod. Phys.* **82**, 1155 (2010).
- [22] E. A. Novikov, Functionals and the random-force method in turbulence theory, *Sov. Phys. JETP* **20**, 1290 (1965).
- [23] A. A. Budini, Quantum systems subject to the action of classical stochastic fields, *Phys. Rev. A* **64**, 052110 (2001).
- [24] A. Insinga, B. Andresen, P. Salamon, and R. Kosloff, Quantum heat engines: Limit cycles and exceptional points, *Phys. Rev. E* **97**, 062153 (2018).
- [25] S. Deffner, C. Jarzynski, and A. del Campo, Classical and quantum shortcuts to adiabaticity for scale-invariant driving, *Phys. Rev. X* **4**, 021013 (2014).
- [26] D. Guéry-Odelin, A. Ruschhaupt, A. Kiely, E. Torrontegui, S. Martínez-Garaot, and J. G. Muga, Shortcuts to adiabaticity: Concepts, methods, and applications, *Reviews of Modern Physics* **91**, 045001 (2019).
- [27] M. V. Berry, Transitionless quantum driving, *Journal of Physics A: Mathematical and Theoretical* **42**, 365303 (2009).
- [28] T. Feldmann and R. Kosloff, Quantum lubrication: Suppression of friction in a first-principles four-stroke heat engine, *Phys. Rev. E* **73**, 025107 (2006).
- [29] P. Pietzonka and U. Seifert, Universal trade-off between

- power, efficiency, and constancy in steady-state heat engines, *Phys. Rev. Lett.* **120**, 190602 (2018).
- [30] T. Denzler and E. Lutz, Efficiency fluctuations of a quantum heat engine, *Phys. Rev. Res.* **2**, 032062 (2020).
- [31] J. M. Horowitz and T. R. Gingrich, Thermodynamic uncertainty relations constrain non-equilibrium fluctuations, *Nature Physics* **16**, 15 (2020).
- [32] G. T. Landi and M. Paternostro, Irreversible entropy production: From classical to quantum, *Rev. Mod. Phys.* **93**, 035008 (2021).
- [33] D. Reiche, J.-T. Hsiang, and B.-L. Hu, Quantum thermodynamic uncertainty relations, generalized current fluctuations and nonequilibrium fluctuation–dissipation inequalities, *Entropy* **24**, 1016 (2022).
- [34] S. Saryal and B. K. Agarwalla, Bounds on fluctuations for finite-time quantum otto cycle, *Phys. Rev. E* **103**, L060103 (2021).
- [35] A. M. Timpanaro, G. Guarnieri, J. Goold, and G. T. Landi, Thermodynamic uncertainty relations from exchange fluctuation theorems, *Phys. Rev. Lett.* **123**, 090604 (2019).
- [36] G. Manzano, J. M. Horowitz, and J. M. R. Parrondo, Nonequilibrium potential and fluctuation theorems for quantum maps, *Phys. Rev. E* **92**, 032129 (2015).
- [37] H. J. D. Miller, M. H. Mohammady, M. Perarnau-Llobet, and G. Guarnieri, Thermodynamic uncertainty relation in slowly driven quantum heat engines, *Phys. Rev. Lett.* **126**, 210603 (2021).
- [38] U. Fano, Ionization yield of radiations. ii. the fluctuations of the number of ions, *Physical Review* **72**, 26 (1947).
- [39] K. Funo, J.-N. Zhang, C. Chatou, K. Kim, M. Ueda, and A. Del Campo, Universal work fluctuations during shortcuts to adiabaticity by counterdiabatic driving, *Physical Review Letters* **118**, 100602 (2017).
- [40] A. Levy, A. Kiely, J. G. Muga, R. Kosloff, and E. Torrontegui, Noise resistant quantum control using dynamical invariants, *New Journal of Physics* **20**, 025006 (2018).
- [41] A. A. Budini, Non-markovian gaussian dissipative stochastic wave vector, *Phys. Rev. A* **63**, 012106 (2000).